PAPER • OPEN ACCESS

Stark-localization as a probe of nanostructure geometry

New Journal of Physics
The open access journal at the forefront of physics

Deutsche Physikalische Gesellschaft DPG
IOP Institute of Physics

Published in partnership with: Deutsche Physikalische Gesellschaft and the Institute of Physics

OPEN ACCESS

RECEIVED
3 May 2022

REVISED
3 August 2022

ACCEPTED FOR PUBLICATION
19 August 2022

PUBLISHED
29 September 2022

PAPER

Stark-localization as a probe of nanostructure geometry

T G Pedersen[1,*], H D Cornean[2], D Krejčiřík[3], N Raymond[4] and E Stockmeyer[5]

[1] Department of Materials and Production, Aalborg University, DK-9220 Aalborg Øst, Denmark
[2] Department of Mathematical Sciences, Aalborg University, DK-9220 Aalborg Øst, Denmark
[3] Department of Mathematics, Faculty of Nuclear Sciences and Physical Engineering, Czech Technical University in Prague, Trojanova 13, 12000 Prague 2, Czech Republic
[4] Laboratoire Angevin de Recherche en Mathématiques, LAREMA, UMR6093, UNIV Angers, SFR Math-STIC, 2 boulevard Lavoisier 49045 Angers Cedex 01, France
[5] Instituto de Física, Pontificia Universidad Católica de Chile, Vicuña Mackenna 4860, Santiago 7820436, Chile
[*] Author to whom any correspondence should be addressed.

E-mail: tgp@mp.aau.dk

Keywords: nanostructures, Stark, spectroscopy

Abstract

It is a central tenet of quantum mechanics that spatial resolution is limited by the wave nature of particles. Energies of stationary states reflect delocalized wave functions and cannot be ascribed to any single point. Yet, electrons confined in nanostructures become localized against the boundary by strong electric fields. Energies then reflect the local curvature of the nanostructure surface rather than entire volume. We propose using spectroscopy of Stark-localized states to map nanostructure surface curvature. By varying field direction, local curvatures are extracted from absorption spectra. Moreover, the required field strength is shown to be feasible experimentally. We use nanowires with elliptic cross section as a detailed benchmark providing quantitative error estimates and practical guide lines.

1. Introduction

Optical spectroscopy is among the most useful techniques for characterization of nanostructures [1–3]. Both energy levels and symmetry properties are revealed by various optical probes. Nanostructures suspended in vacuum or air are characterized by tall barriers confining electrons to their interior [1–5]. In turn, electrons and holes in the interior behave essentially as free particles except that their apparent mass is the effective one. As a consequence, electron and hole eigenstates are solutions of the Helmholtz equation. Their eigenvalues are, therefore, properties of the entire surface bounding the nanoparticle. Kac famously asked 'can you hear the shape of a drum?' in relation to the equivalent problem of a vibrating membrane [6]. The answer turned out to be 'no' since knowing all eigenvalues is not enough to uniquely determine shape. Knowing only part of the spectrum leads to even greater shape uncertainty. The question we ask in the present work is whether or not optical spectroscopy can determine nanostructure surface geometries. As with the vibrating drum, the answer is clearly 'no' if only surfaces restrict eigenstates. Electrons, however, differ from drums by being highly sensitive to strong electric fields. In the present work, we propose using the Stark effect in strong electric fields to facilitate local probes of the nanostructure geometry. Thus, a sufficiently strong Stark field will push electrons and holes against the barrier and, in turn, a weak infrared field probing transitions between Stark-localized states will reveal the local surface curvature. By varying the direction of the Stark field, a full mapping of the curvature is possible.

The envisioned experimental setup is sketched in figure 1. We focus on translationally invariant nanowires in a transverse Stark field, cf figure 1(a). In addition, a weak optical probe field is present. The polarization of the probe field must have a component perpendicular to both Stark field and nanowire long-axis in order to probe transitions between confined states as shown in figure 1(b). Note that this setup would apply equally well to two-dimensional islands and patches such as graphene nanodisks [7] subject to in-plane fields. A strong Stark field will pull electrons and push holes against the barrier, respectively. The stronger the field, the more tightly confined the carriers. Eventually, states cease to be delocalized over the

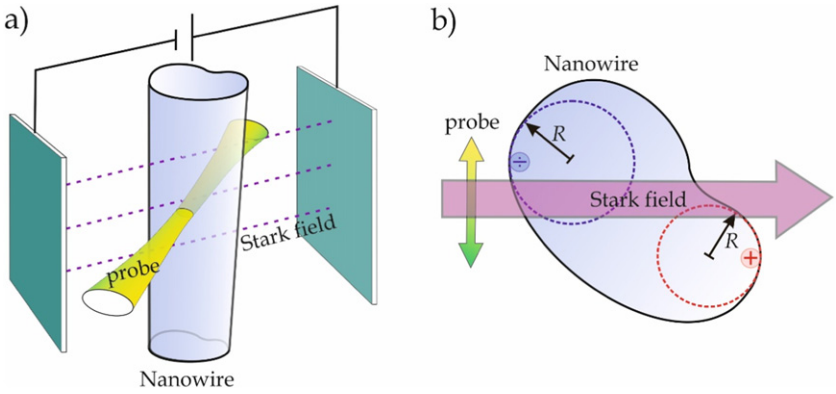

Figure 1. (a) Schematic setup showing a nanowire in a strong Stark field and weak infrared probe field. (b) The Stark field pushes carriers against the boundary, such that resonant absorption of a perpendicular probe field becomes sensitive to local radius of curvature R. Electrons (blue) and holes (red) Stark-localize on opposite sides.

entire cross section but, instead, find themselves confined by the field and the barrier at the point of maximal Stark effect on the nanowire boundary, as sketched in figure 1(b). Electrons and holes are, thus, Stark-localized near points on the boundary with maximum displacement in the negative and positive field direction, respectively. Importantly, confinement in the in-plane direction perpendicular to the Stark field is governed by the local curvature. Thus, a small radius of curvature translates into tight confinement in the perpendicular dimension, see figure 1(b). The final ingredient in our proposal is the probe field inducing transitions between Stark-localized states. As is intuitively clear, such transitions will be highly sensitive to the local curvature. In fact, as recently demonstrated [8], the system behaves mathematically as a harmonic oscillator with characteristic frequency determined by the curvature radius R. By scanning the Stark field direction (or rotating the nanowire), the local curvature along the boundary may finally be mapped.

Our proposal is quite generic but, still, has obvious limitations. Primarily, only convex boundaries can be mapped in entirety. Any locally concave points, i.e. points intersected by lines joining other boundary points, cannot be probed because such points never support Stark-localized states. More subtly, our proposal rests on the assumption that barriers between nanowire and surroundings are sufficiently tall that carriers remain confined even in large Stark fields, that is, barriers effectively acting as hard walls. Hence, our proposal applies to free-standing nanowires with a substantial barrier between interior and exterior, as opposed to heterostructures with barriers formed by varying atomic composition. High quality free-standing nanowires have been demonstrated in a wide range of materials, see e.g. [9–11]. Below, the infinite-barrier approximation will be critically examined. As a realistic benchmark, we consider nanowires with an elliptic cross section. From simulated probe absorption spectra in strong Stark fields in this geometry, we demonstrate that our proposal is, indeed, feasible. We consequently expect that spectroscopic studies of Stark-localized electronic states will pave the way for a novel toolbox of significance for nanostructure characterization.

2. Stark-localization

We now introduce the model applied to describe Stark-localization on the boundary of a two-dimensional domain. The Stark field $\vec{F}$ can take arbitrary orientations within the plane of the domain. For definiteness, we consider electrons but all considerations apply equally to holes. We assume carriers are introduced via doping in contrast to interband photo-excitation, which produces electron–hole pairs. Consequently, electron–hole interactions are not considered. Moreover, we assume that the semiconductor is characterized by an isotropic effective mass m^* in the cross-sectional plane (x, y). In a translationally invariant nanowire, states are of the form $\varphi(x, y)e^{ikz}$ with an in-plane part $\varphi(x, y)$ determined by

$$\left\{-\frac{\hbar^2}{2m^*}\nabla^2 + e\vec{F}\cdot\vec{r}\right\}\varphi(\vec{r}) = E\varphi(\vec{r}). \tag{1}$$

This equation is supplemented by Dirichlet boundary conditions $\varphi(\vec{r}) = 0$ on the boundary $\partial\Omega$ of the domain, i.e. nanowire cross section. Formally, Dirichlet boundary conditions correspond to an infinite barrier between interior and exterior. Physically, this barrier is the electron affinity of the semiconductor material surrounded by vacuum. As an example, this barrier V is about 4 eV in GaAs and similar inorganic semiconductors [12]. If the characteristic dimension ('diameter') of the cross section is L, it follows that

Dirichlet boundary conditions apply approximately if $eFL \ll V$. This places an upper limit on the acceptable field strength. A second concern is the dielectric breakdown limit reached by sufficiently high fields. Both of these restrictions are analyzed in more detail below.

In any inversion-symmetric geometry, the lowest field-dependent correction to the energy is quadratic. In terms of the nanostructure polarizability tensor $\overleftrightarrow{\alpha}$, see references [13–20], we have $E(\vec{F}) = E(0) - \frac{1}{2}\vec{F}\cdot\overleftrightarrow{\alpha}\cdot\vec{F} + O(F^4)$. The in-plane nanowire polarizability takes a diagonal form $\overleftrightarrow{\alpha} = \mathrm{diag}(\alpha_{xx}, \alpha_{yy})$ in the principal-axis system, with axes coinciding with mirror lines in symmetric cases such as ellipses. In general, some geometric information is contained in $\overleftrightarrow{\alpha}$. Thus, a tightly confined principal direction implies a reduced polarizability element. Similarly, highly symmetric cross sections such as circles [21], hexagons and squares [22] lead to isotropic polarizability tensors. It follows that angle-resolved low-field Stark spectroscopy provides useful geometric information about symmetries and nanowire aspect ratio. However, it is clear that only limited detail may be extracted from a single pair of numbers $(\alpha_{xx}, \alpha_{yy})$. If more elaborate geometry mapping is desired in Stark spectroscopy, strong fields beyond the quadratic regime are inevitable. Such intense fields drive electrons into regions, where the dipole energy $e\vec{F}\cdot\vec{r}$ is minimum. We denote the location on the boundary corresponding to the minimum by $\vec{r}_{\min}$. In the extreme high-field limit, we have previously shown [8] that the low lying energies satisfy

$$E(\vec{F}) = e\vec{F}\cdot\vec{r}_{\min} - z_1\left(\frac{\hbar^2 e^2 F^2}{2m^*}\right)^{1/3} + \left(\frac{\hbar^2 eF\kappa}{m^*}\right)^{1/2}(\nu - \frac{1}{2}) + O(F^{1/3}), \tag{2}$$

where $z_1 = 2.338\,107\,410\,46\ldots$ is the first zero of the Airy function $\mathrm{Ai}(-z)$ and ν is a positive integer. Crucially, $\kappa = R^{-1}$ in this expression is the local curvature at $\vec{r}_{\min}$. Physically, the curvature term follows from a harmonic oscillator describing motion along the boundary in the vicinity of $\vec{r}_{\min}$. The potential energy cost associated with displacement from $\vec{r} = \vec{r}_{\min}$ increases with both field strength and curvature. It follows that a convex boundary forces electrons to move against the electric force as they oscillate about $\vec{r}_{\min}$. As seen from equation (2), the harmonic oscillator frequency $\omega_0 = (eF\kappa/m^*)^{1/2}$ increases as the square-root $(F\kappa)^{1/2}$ of the product of field and curvature. A weak optical probe with a frequency ω will be resonantly absorbed if $\omega \approx \omega_0$ such that an absorption spectrum provides direct access to the curvature κ. We stress the crucial point that ω_0 depends *only* on curvature implying that geometry can be determined in a model-independent way in the high-field regime.

3. Elliptical nanowires

As already mentioned, we will use nanowires with elliptical cross section, such as the one in the inset of figure 2, as a detailed benchmark and proof of concept. Elliptic boundaries are convenient because they are convex, smooth and easily adjustable through their major and minor axes a and b corresponding to an aspect ratio $\eta = a/b$. The electric field $\vec{F}$ is at an angle θ to the major axis. We simulate the strong-field Stark response numerically by transforming to a circular domain through the scaling $x \to x/a$ and $y \to y/b$. In this manner, the confinement is circular at the expense of an anisotropic Laplacian, and we have

$$\left\{-\frac{\hbar^2}{2m^*a^2}\frac{\mathrm{d}^2}{\mathrm{d}x^2} - \frac{\hbar^2}{2m^*b^2}\frac{\mathrm{d}^2}{\mathrm{d}y^2} + eaF_x x + ebF_y y\right\}\varphi(\vec{r}) = E\varphi(\vec{r}), \qquad \partial\Omega : x^2 + y^2 = 1. \tag{3}$$

A convenient dimensionless form is found if we introduce $E_0 \equiv \hbar^2/(m^*b^2)$ as well as $\varepsilon = E/E_0$ and $\vec{\mathcal{E}} = eb\vec{F}/E_0$. Hence, as a result,

$$\left\{-\frac{1}{2\eta^2}\frac{\mathrm{d}^2}{\mathrm{d}x^2} - \frac{1}{2}\frac{\mathrm{d}^2}{\mathrm{d}y^2} + \eta\mathcal{E}_x x + \mathcal{E}_y y\right\}\varphi(\vec{r}) = \varepsilon\varphi(\vec{r}). \tag{4}$$

Furthermore, in terms of the normalized energy $\varepsilon = \varepsilon(\eta, \mathcal{E}_x, \mathcal{E}_y)$, an exact scaling relation $\varepsilon(\eta^{-1}, \eta^3\mathcal{E}_y, \eta^3\mathcal{E}_x) = \eta^2\varepsilon(\eta, \mathcal{E}_x, \mathcal{E}_y)$ is readily established. This relation can be viewed as the result of a rotation by 90 degrees. The exact field-free solutions of equations (3) and (4) are known in terms of Mathieu functions and their characteristics [23, 24]. Since these cannot be expressed in terms of standard functions, such exact solutions are of limited use for the present purposes. As an alternative, one may consider ellipses that only deviate slightly from circles. Thus, for the normalized ground state energy $\varepsilon^{(0)}(\eta)$, in the limit of low ellipticity [25, 26],

$$\varepsilon^{(0)}(\eta) = \frac{\lambda^2}{2} - \frac{\lambda^2}{2}(\eta - 1) + \frac{\lambda^2(6 + \lambda^2)}{16}(\eta - 1)^2 + O[(\eta - 1)^3]. \tag{5}$$

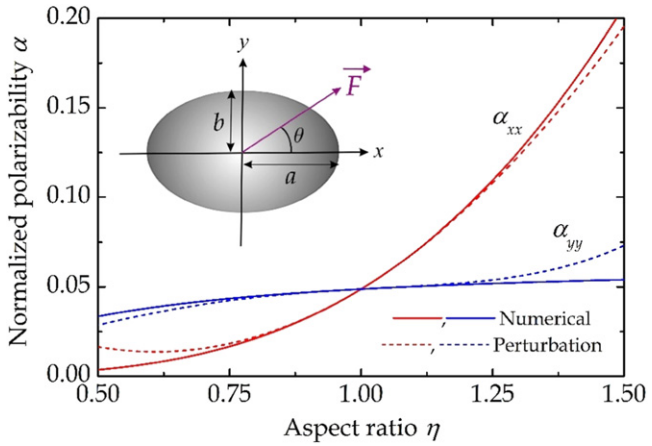

Figure 2. Comparison of numerical (solid lines) and perturbative (dashed lines) Cartesian polarizabilities for an ellipse. Inset: cross section of an ellipse with major and minor axes a and b in an electric field.

Here, $\lambda \equiv \lambda_{01} \approx 2.404\,83$ is the first zero of the 0th Bessel function. Such expansions are useful in the low-field Stark regime, as we demonstrate below. In strong fields, however, eigenstates deviate substantially from unperturbed ones, even for nearly circular domains. Accordingly, an accurate numerical approach based on expansion of Stark-localized eigenstates in a large basis is used throughout. In the appendix, we describe the basis and matrix elements applied to find eigenstates for arbitrary fields. Briefly, eigenstates of an isotropic circular cylinder are selected as a numerical basis. These states are labeled by angular momentum l and radial quantum number n. In all simulations, l and n are restricted to the ranges $-30 \leqslant l \leqslant 30$ and $1 \leqslant n \leqslant 30$, respectively. Hence, the ground state energy $\lambda^2/2$ of a circular nanowire with $\eta = 1$ is reproduced exactly in this basis. The ground state is a special case of the general eigenvalue $\varepsilon_{nl}^{(0)} = \lambda_{ln}^2/2$, where λ_{ln} is the nth zero the lth Bessel function, contained in this basis.

Before investigating the strong-field Stark regime, we briefly discuss the more common weak-field case. This is the regime, in which the electric field may be seen as a weak perturbation, shifting each energy level by a small amount compared to the characteristic spacing between unperturbed levels. In an inversion-symmetric geometry, the shift is quadratic in the field and we find for the ground state

$$\varepsilon(\eta, \mathcal{E}_x, \mathcal{E}_y) = \varepsilon^{(0)}(\eta) - \frac{1}{2}\alpha_{xx}(\eta)\mathcal{E}_x^2 - \frac{1}{2}\alpha_{yy}(\eta)\mathcal{E}_y^2 + O(\mathcal{E}^4). \tag{6}$$

The exact scaling relation implies that $\alpha_{xx}(\eta) = \eta^4\alpha_{yy}(\eta^{-1})$ and $\alpha_{yy}(\eta) = \eta^4\alpha_{xx}(\eta^{-1})$. In the case of a perfect circle, it is known [21] that $\alpha_{xx}(1) = \alpha_{yy}(1) = (4 + \lambda^2)/(6\lambda^4) \equiv \alpha_0$. A tedious perturbation expansion leads to the results

$$\begin{aligned}\alpha_{xx}(\eta) &= \alpha_0 + (\eta - 1)\alpha_1 + (\eta - 1)^2\alpha_2 + O[(\eta - 1)^3],\\ \alpha_{yy}(\eta) &= \alpha_0 + (\eta - 1)(4\alpha_0 - \alpha_1) + (\eta - 1)^2(6\alpha_0 - 3\alpha_1 + \alpha_2) + O[(\eta - 1)^3].\end{aligned} \tag{7}$$

Here,

$$\alpha_1 = \frac{1}{8} + \frac{16 + \lambda^2}{12\lambda^4} \approx 3.6772\alpha_0, \qquad \alpha_2 = \frac{7}{24} - \frac{5}{24\lambda^2} + \frac{1}{\lambda^4} + \frac{1}{8(\lambda^2 - 8)} \approx 4.7004\alpha_0. \tag{8}$$

The numerical magnitude of these corrections shows that, in fact, the polarizabilities are sensitive probes of the global geometry. The comparison in figure 2 demonstrates that the perturbative results equation (7) hold to good accuracy in the range $0.75 < \eta < 1.25$. Even in this restricted range, a significant variation in polarizability is observed. In particular, the results show that the major-axis component $\alpha_{xx}(\eta)$ is doubled compared to the case of a circle $\alpha_{xx}(1)$ if the aspect ratio is increased to $\eta \approx 1.21$. Hence, slight geometric deformations lead to substantial changes in the Stark shift. Also, it is apparent that the *ratio* $\alpha_{xx}(\eta)/\alpha_{yy}(\eta)$ is a sensitive measure of aspect ratio, obviating absolute measurement of dimensions.

Next, we turn to the strong-field regime in order to validate the expansion equation (2). Specifically, we wish to determine the field strength required for the harmonic oscillator term to describe the ground state and lowest excitations with acceptable accuracy. Similarly to the normalization applied above, we introduce

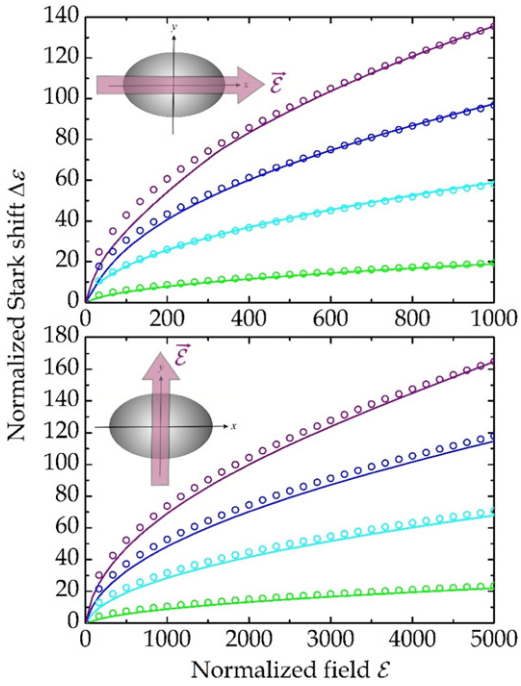

Figure 3. Energy shift $\Delta\varepsilon$ for the four lowest levels in horizontal (top) and vertical (bottom) Stark fields. Solid curves are numerical diagonalization results while circles are analytical harmonic oscillator predictions. The ellipse aspect ratio is $\eta = 1.5$.

a normalized curvature $\tilde{\kappa} = b\kappa$. Thus, in terms of normalized quantities, the strong-field expansion takes on a particularly simple form

$$\varepsilon(\vec{\mathcal{E}}) = \vec{\mathcal{E}} \cdot \vec{r}_{\min}/b - z_1\left(\frac{1}{2}\mathcal{E}^2\right)^{1/3} + (\tilde{\kappa}\mathcal{E})^{1/2}\left(n - \frac{1}{2}\right) + O(\mathcal{E}^{1/3}). \tag{9}$$

The curvature $\kappa = R^{-1}$ of an ellipse is $(a^2\cos^2\theta + b^2\sin^2\theta)^{3/2}/(ab)^2$ so that, conveniently, $\tilde{\kappa} = (\eta^2\cos^2\theta + \sin^2\theta)^{3/2}/\eta^2$. We first compare the numerical solutions to equation (4) with the expansion equation (9). To this end, we apply the Bessel basis as described above and consider the Stark shift $\Delta\varepsilon \equiv \varepsilon(\vec{\mathcal{E}}) - \varepsilon(0) - \vec{\mathcal{E}} \cdot \vec{r}_{\min}/b + z_1(\frac{1}{2}\mathcal{E}^2)^{1/3}$. Here, the two universal terms in equation (9) were subtracted so that the dominant part of $\Delta\varepsilon$ is the harmonic oscillator term varying as the square-root of the field strength. The prefactor $\tilde{\kappa}$ means, however, that the magnitude of this term depends on orientation of the field. Generally, low-curvature directions require larger fields in order to fully dominate subleading terms. For the ellipse, a ratio of η^3 is found between horizontal and vertical prefactors $\tilde{\kappa}$.

For numerical benchmarking, we select an ellipse with an aspect ratio of $\eta = 1.5$. Accordingly, a simple expectation for the critical fields required to enter the strong-field regime would be that vertical fields exceed horizontal ones by a factor $1.5^3 \approx 3.4$. In figure 3, we compare the analytical harmonic oscillator expression $(\tilde{\kappa}\mathcal{E})^{1/2}(\nu - \frac{1}{2})$ to numerical values of $\Delta\varepsilon$ in strong fields. It is immediately clear that the numerical high-field behavior follows a square-root dependence to good accuracy. However, examining the curves more carefully, we find discrepancies that depend on field strength and orientation. In relatively weak fields, the harmonic oscillator result overestimates the actual eigenvalues. In the case of a horizontal field shown in the top panel of figure 3, a normalized field of about $\mathcal{E} = 1000$ is required to limit deviations to approximately 3% for the energy difference between the two lowest states. In the vertical case, shown in the bottom panel, the field must be significantly larger in agreement with the curvature-based arguments above. It must be noted, however, that our proposal rests on the accuracy of energy *differences* probed by absorption spectroscopy. Thus, systematic errors common to all levels are of no consequence. Below, the error associated with transition energies is estimated.

As mentioned in the introduction, the assumption of Dirichlet boundary conditions corresponding to infinite barriers is only valid if $F \ll V/(eL)$, where V is the actual surface barrier. In terms of the normalized field and taking $L = b$, this requirement is conveniently expressed as

$$\mathcal{E} \ll \frac{V}{\mathrm{Ha}} \times \frac{b^2}{a_0^2} \times \frac{m^*}{m_0}, \tag{10}$$

where Ha ≈ 27.21 eV is the Hartree energy, a_0 is the Bohr radius, and m_0 is the free electron mass. The conduction band in GaAs can be seen as an extreme case due to the exceedingly small effective mass [1–3] $m^* \approx 0.067 m_0$. Thus, with $V = 4$ eV, a field of $\mathcal{E} = 1000$ translates into a requirement $b \gg 17$ nm. Hence, for nanowires in the 10 nm range, such fields will lead to inaccuracies since the finite confinement barrier can no longer be ignored. In most materials, however, the effective mass is larger leading to relaxed restrictions. For a 40 nm radius GaAs nanowire, the characteristic confinement energy is $E_0 = \hbar^2/(m^* b^2) \approx 0.7$ meV. This means that the GaAs dielectric breakdown limit [27] around 30 MV m^{-1} is reached with a normalized field of approximately $\mathcal{E} = 1700$, placing a strict upper limit on the applicable field. We stress that the Stark field is static in our setup, thereby suppressing photoemission across the surface barrier, which is known to occur in intense time-dependent (pulsed) fields [28].

Throughout, we have ignored Coulomb interactions between the conduction electrons. At a sufficiently high density, this simplification will be invalid. To quantify this restriction, we consider a nanowire with a finite electron density ρ per unit length and require $\rho a_{\mathrm{HO}} \ll 1$, where $a_{\mathrm{HO}} = \hbar^{1/2}/(m^* eF\kappa)^{1/4}$ is the characteristic confinement length of the harmonic oscillator, as derived from equation (2), and ρ^{-1} is a measure of the average electron–electron separation. This requirement ensures that many-body effects are negligible compared to differences between Stark shifts and translates into a lower bound for the Stark field $F_{\mathrm{L}} = \hbar^2 \rho^4/(m^* e\kappa)$. Similarly to the analysis above, we again consider a GaAs nanowire with radius $b = 40$ nm. Thus, taking $\kappa = b^{-1}$ as well as $\rho = b^{-1}$, corresponding to electrons separated approximately by the nanowire radius, we find a rather small lower bound of $F_{\mathrm{L}} \approx 18$ kV m^{-1}. We note that GaAs is an extreme case due to its diminutive effective mass. However, the ρ^4 scaling means that, eventually, Coulomb corrections will be of importance for more highly doped materials, even if the bound is reduced by a larger effective mass.

4. Stark spectroscopy

A weak probe field of the form $F_\omega \cos\omega t$ will induce transitions between Stark-localized states. This will manifest itself as scattering or absorption of the probe beam. From an analysis of scattering or absorption resonances, transition energies $E_{\nu\mu} = E_\nu - E_\mu$ may be inferred. For the ideal harmonic oscillator, only $\nu = \mu \pm 1$ transitions are allowed and $\omega = \omega_0$ the only resonance observed. We expect this simple picture to emerge in strong fields, while a much more intricate spectral response is expected in weak fields. Absorption of the probe field is described by the imaginary part of the frequency-dependent polarizability $\alpha(\omega)$, while scattering is governed by the absolute value. If the probe field is polarized at 45 degrees to a principal axis, transitions along both axes are probed. In this case, the polarizability of an electron in the ground state $|1\rangle$ is [19]

$$\alpha(\omega) = e^2 \sum_\nu E_{\nu 1} \frac{|\langle 1|x|\nu\rangle|^2 + |\langle 1|y|\nu\rangle|^2}{E_{\nu 1}^2 - \hbar^2\omega^2}. \tag{11}$$

The dipole matrix elements $\langle 1|\vec{r}|\nu\rangle$ are readily expanded in the Bessel basis using equation (A4). The response equation (11) only captures absorption by dopant electrons. Realistically, a bulk contribution, both electronic and vibrational, should be added. Hence, transitions between Stark-localized states will appear on top of a background signal.

We envision rotating the nanowire in the Stark field while recording the probe absorption spectrum. The lowest resonance E_{21} should ideally be a direct measure of the curvature following the harmonic oscillator relation $E_{21} = \hbar(eF\kappa/m^*)^{1/2}$. In order to assess the accuracy of this relation, we have simulated absorption spectra using finite fields oriented at various angles to the nanowire major axis. For simplicity, we work in normalized units such that ideally $\varepsilon_{21} = (\tilde{\kappa}\mathcal{E})^{1/2}$ or, equivalently, $\tilde{\kappa} = \varepsilon_{21}^2/\mathcal{E}$ for the harmonic oscillator. Also, the dynamic polarizability is expressed in units of $e^2b^2/E_0 = e^2b^4m^*/\hbar^2$. The fourth-power scaling with dimensions is characteristic of polarizabilities in effective-mass theories [16–20]. We must distinguish between the *actual* geometric curvature $\tilde{\kappa}$ and the *inferred* curvature $\varepsilon_{21}^2/\mathcal{E}$ derived from absorption resonances. Only in the limit of extremely large fields will the two agree. From a comparison at various finite field strengths we may then quantify the inherent error associated with the inferred curvature.

In figure 4, we present simulated absorption spectra for normalized Stark fields $\mathcal{E}$ of magnitude 100 and 1000, oriented at various angles to the ellipse major axis a taking, again, $\eta = 1.5$. The photon frequency ω is normalized by E_0, i.e. we substitute $\hbar\omega/E_0 \to \omega$ and, moreover, a finite line width is included by adding an imaginary term $\mathrm{i}/2$ to ω. The top and bottom panels in figure 4 illustrate cases of moderate and strong Stark fields, respectively. If $\mathcal{E} = 100$, the Stark shift is not quite in the harmonic oscillator limit. As a consequence, the absorption spectra contain several resonances that shift with orientation of the Stark field. In contrast, if $\mathcal{E} = 1000$, each spectrum essentially consists of a single peak. An example of the transition responsible for this peak is shown in the figure inset in figure 4, bottom panel. Here, the ground and first

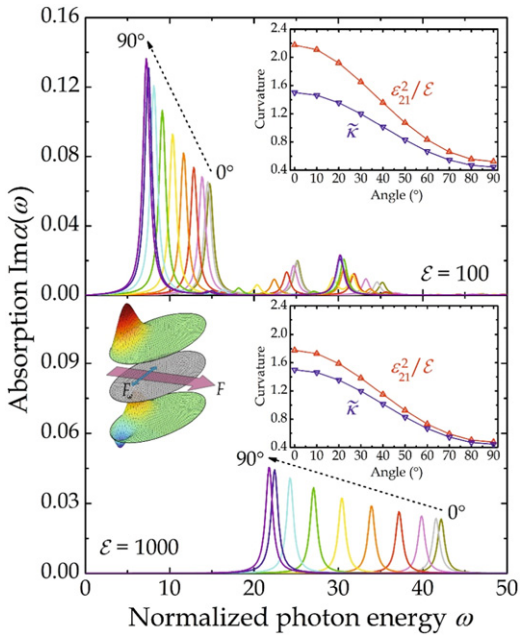

Figure 4. Simulated probe absorption in cases of moderate ($\mathcal{E} = 100$, top panel) and strong ($\mathcal{E} = 1000$, bottom panel) Stark fields. Different orientations of the Stark field between 0° and 90° are indicated by color. The graph insets compare the inferred and actual curvatures vs angle. Also, the bottom figure inset illustrates ground and first excited Stark-localized states.

excited Stark-localized states are shown. It is clear that the transition dipole is perpendicular to the Stark field such that a perpendicular component in the probe field is required.

We now turn to the curvatures inferred from the resonances $\varepsilon_{21}^2/\mathcal{E}$ in the absorption spectra. These are shown in red as insets for both moderate and strong Stark fields in figure 4. For comparison, the actual geometric curvature $\tilde{\kappa}$ is shown as blue symbols. As is apparent from the insets, the inferred curvature tends to overestimate the actual one. This is especially pronounced is the moderate field case, while the error decreases in the strong field. Numerically, the maximum error for $\mathcal{E} = 1000$ is approximately 18% with a decreasing tendency towards larger angles, reaching 7% at 90° orientation. Overall, the inferred curvature manages to capture the exact angular dependence rather accurately, but quantitative agreement clearly requires large Stark fields, as expected.

5. Summary

We have suggested probing transitions between Stark-localized states in nanostructures as a tool for mapping surface curvature. Physically, a strong Stark field pushes carriers against the surface barrier such that any motion perpendicular to the field is sensitive to the local curvature. In turn, a weak time-dependent probe induces transitions between Stark-localized states. Finally, an analysis of probe absorption spectra provides the inferred curvature. Using nanowires with elliptic cross sections as benchmarks, we have examined the feasibility of our proposal. While weak fields allow for probes of global properties such as nanowire aspect ratio, a strong field is found to provide much more detailed geometric information. We establish criteria for the required field strength demonstrating that our proposal is, indeed, realistic. Finally, an assessment of curvature inferred from probe absorption spectra shows that local geometric information can be obtained with reasonable accuracy.

Acknowledgments

DK has been supported by the EXPRO Grant No. 20-17749X of the Czech Science Foundation (GAČR). ES has been partially funded by Fondecyt (Chile) project #118–0355.

Data availability statement

All data that support the findings of this study are included within the article (and any supplementary files).

Appendix. Cylindrical Bessel basis

As described in the main text, we transform to a circular domain at the expense of introducing an anisotropic Laplacian. Moreover, coordinates are scaled such that the radius of the circular domain is unity. As a convenient normalized basis, we choose the Bessel eigenstates of a circle with isotropic Laplacian

$$\varphi^{(0)}_{nl}(\vec{r}) = \frac{\mathrm{e}^{\mathrm{i}l\theta}J_l(\lambda_{ln}r)}{\sqrt{\pi}J_{l+1}(\lambda_{ln})}, \qquad \varepsilon^{(0)}_{nl} = \frac{\lambda^2_{ln}}{2}. \tag{A1}$$

Here, J_l the lth Bessel function, for which λ_{ln} is the nth zero, i.e. $J_l(\lambda_{ln}) = 0$ with eigenstate index $n = 1, 2, 3, \ldots$. Moreover, $\varepsilon^{(0)}_{nl}$ is the normalized energy eigenvalue. We require matrix elements for both kinetic energies and Stark terms. Thus, between states with identical angular momentum l

$$\left\langle \varphi^{(0)}_{nl}\middle|\frac{\mathrm{d}^2}{\mathrm{d}x^2}\middle|\varphi^{(0)}_{ml}\right\rangle = \left\langle \varphi^{(0)}_{nl}\middle|\frac{\mathrm{d}^2}{\mathrm{d}y^2}\middle|\varphi^{(0)}_{ml}\right\rangle = -\frac{1}{2}\lambda^2_{ln}\delta_{nm}, \tag{A2}$$

while the corresponding off-diagonal block $l' \neq l$ is

$$\left\langle \varphi^{(0)}_{nl}\middle|\frac{\mathrm{d}^2}{\mathrm{d}x^2}\middle|\varphi^{(0)}_{ml'}\right\rangle = -\left\langle \varphi^{(0)}_{nl}\middle|\frac{\mathrm{d}^2}{\mathrm{d}y^2}\middle|\varphi^{(0)}_{ml'}\right\rangle = \mathrm{sgn}(l'-l)(l+l')\frac{\lambda_{ln}\lambda_{l'm}}{2(\lambda^2_{l'm}-\lambda^2_{ln})}. \tag{A3}$$

Similarly, the dipole matrix elements are [20]

$$\left\langle \varphi^{(0)}_{nl}(\vec{r})\middle|x\middle|\varphi^{(0)}_{ml'}(\vec{r})\right\rangle = \delta_{l',l\pm1}\frac{\lambda_{ln}\lambda_{l'm}}{(\lambda^2_{ln}-\lambda^2_{l'm})^2}, \qquad \left\langle \varphi^{(0)}_{nl}(\vec{r})\middle|y\middle|\varphi^{(0)}_{ml'}(\vec{r})\right\rangle = \mathrm{i}\ \mathrm{sgn}(l-l')\delta_{l',l\pm1}\frac{\lambda_{ln}\lambda_{l'm}}{(\lambda^2_{ln}-\lambda^2_{l'm})^2}. \tag{A4}$$

Based on these matrix elements, the eigenstates in an electric field are found from numerical diagonalization.

ORCID iDs

T G Pedersen https://orcid.org/0000-0002-9466-6190
H D Cornean https://orcid.org/0000-0003-2700-8785

References

[1] Haug H and Koch S W 1993 *Quantum Theory of the Optical and Electronic Properties of Semiconductors* (Singapore: World Scientific)
[2] Basu P K 1997 *Theory of Optical Processes in Semiconductors* (Oxford: Oxford University Press)
[3] Yu P Y and Cardona M 2003 *Fundamentals of Semiconductors* (Berlin: Springer)
[4] Zhu J-L, Xiong J-J and Gu B-L 1990 *Phys. Rev.* B **41** 6001
[5] Kan S, Mokari T, Rothenberg E and Banin U 2003 *Nat. Mater.* **2** 155
[6] Kac M 1966 *Am. Math. Mon.* **73** 1
[7] Gutiérrez C, Brown L, Kim C-J, Park J and Pasupathy A N 2016 *Nat. Phys.* **12** 1069
[8] Cornean H, Krejčiřík D, Pedersen T G, Raymond N and Stockmeyer E 2022 *SIAM J. Math. Anal.* **54** 2114
[9] Banerjee D, Lao J Y, Wang D Z, Huang J Y, Ren Z F, Steeves D, Kimball B and Sennett M 2003 *Appl. Phys. Lett.* **83** 2061
[10] Koblmuller G and Abstreiter G 2014 *Phys. Status Solidi RRL* **8** 11
[11] Kargar F, Debnath B, Kakko J-P, Säynätjoki A, Lipsanen H, Nika D L, Lake R K and Balandin A A 2016 *Nat. Commun.* **7** 13400
[12] Sze S M 1981 *Physics of Semiconductor Devices* (New York: Wiley)
[13] Empedocles S A and Bawendi M G 1997 *Science* **278** 214
[14] Li D, Zhang J, Zhang Q and Xiong Q 2012 *Nano Lett.* **12** 2993
[15] Klein J, Wierzbowski J, Regler A, Becker J, Heimbach F, Müller K, Kaniber M and Finley J J 2016 *Nano Lett.* **16** 1554
[16] Pedersen T G, Latini S, Thygesen K S, Mera H and Nikolić B K 2016 *New J. Phys.* **18** 073043
[17] Pedersen T G 2017 *Phys. Rev.* B **96** 115432
[18] Pedersen T G 2019 *Phys. Rev.* A **99** 063410
[19] Pedersen T G 2021 *Phys. Rev.* B **104** 155414
[20] Szabó P, Góger S, Charry J, Karimpour M R, Fedorov D V and Tkatchenko A 2022 *Phys. Rev. Lett.* **128** 070602
[21] Pedersen T G 2017 *New J. Phys.* **19** 043011

[22] Yi G, Wei G and Wu H 2007 *Phys. Status Solidi b* **244** 4651
[23] Troesch B A and Troesch H R 1973 *Math. Comput.* **27** 755
[24] Magner A G, Fedotkin S N, Arita K, Misu T, Matsuyanagi K, Schachner T and Brack M 1999 *Prog. Theor. Phys.* **102** 551
[25] Joseph D D 1967 *Arch. Ration. Mech. Anal.* **24** 325
[26] Fiore A and Grinfeld P 2010 *Numer. Funct. Anal. Optim.* **31** 679
[27] Luo J K, Thomas H, Morgan D V, Westwood D and Williams R H 1994 *Semicond. Sci. Technol.* **9** 2199
[28] Dombi P *et al* 2020 *Rev. Mod. Phys.* **92** 025003